Au$_2^+$ cannot catalyze conversion of methane to ethene at low temperature: An exploration of the relevant chemistry using selected-ion flow tube, guided ion beam mass spectrometry, and theory

Journal:	*Catalysis Science & Technology*
Manuscript ID	CY-ART-03-2019-000523.R1
Article Type:	Paper
Date Submitted by the Author:	23-Apr-2019
Complete List of Authors:	Shuman, Nicholas; Air Force Research Laboratory, Ard, Shaun; Air Force Research Laboratory, Space Vehicles Directorate; Boston College, Insitute of Scientific Research Sweeny, Brendan; Air Force Research Laboratory Pan, Hanqing; Air Force Research Laboratory Viggiano, Albert; Air Force Research Laboratory, Space Vehicles Directorate Keyes, Nicholas; University of New Mexico, Department of Chemistry Guo, Hua; University of New Mexico, Department of Chemistry Owen, Cameron; University of Utah, Chemistry Armentrout, Peter; University of Utah, Chemistry

SCHOLARONE™
Manuscripts

1

[1]   Au$_2^+$ cannot catalyze conversion of methane to ethene at low temperature: An exploration of the relevant chemistry using selected-ion flow tube, guided ion beam mass spectrometry, and theory

Nicholas S. Shuman,[1] Shaun G. Ard,[2] Brendan C. Sweeny,[3] Hanqing Pan,[4] Albert A. Viggiano,[1] Nicholas R. Keyes,[5] Hua Guo,[5] Cameron J. Owen,[6] and P. B. Armentrout[6]

[1]*Air Force Research Laboratory, Space Vehicles Directorate, Kirtland AFB, NM 87117 USA*
[2]*Institute for Scientific Research, Boston College, Boston, MA 02467 USA*
[3]*National Research Council Research Associateship Program at Air Force Research Laboratory, Space Vehicles Directorate, Kirtland AFB, NM 87117 USA*
[4]*USRA Space Scholar at Air Force Research Laboratory, Space Vehicles Directorate, Kirtland Air Force Base, New Mexico 87117*
Laboratory, Space Vehicles Directorate, Kirtland AFB, NM 87117 USA
[5]*Department of Chemistry and Chemical Biology, University of New Mexico, Albuquerque, NM 87131 USA*
[6]*Department of Chemistry, University of Utah, Salt Lake City, Utah 84112, USA*

Abstract

The previously reported conversion of methane to ethene catalyzed by Au$_2^+$ at thermal energies, at odds with established thermodynamics, is investigated through a combination of experiments under both single-collision conditions using a guided ion beam tandem mass spectrometer (GIBMS) apparatus and at higher pressures using a selected-ion flow tube (SIFT) apparatus, as well as through density functional calculations. Production of Au$_2$(C$_2$H$_4$)$^+$ (or *m/z* 422) or Au$_2$(C$_2$D$_4$)$^+$ (or *m/z* 426) is significantly lower in the higher pressure SIFT experiments relative to previously reported results. The amount observed is consistent with a pathway initiating from a small fraction of a reactive species, potentially electronically excited Au$_2^+$* or Au$_2$O$^+$, isobaric with Au$_2$(CH$_4$)$^+$. Extensive theoretical exploration of the potential energy surface for Au$_2$(CH$_4$)$^+$ + CH$_4$ shows no low-energy pathway that is consistent with ethene formation, with prohibitive barriers of 1 - 2 eV calculated along all identified reaction coordinates, consistent with previous calculations. GIBMS data do show the production of *m/z* 422 in the reaction of Au$_2$(CH$_4$)$^+$ +

CH_4, consistent with the proposed key intermediate, but also provide evidence that this observed species is $Au_2(CO)^+$ arising from Au_2O^+, not $Au_2(C_2H_4)^+$ arising from $Au_2(CH_4)^+$. The present results are consistent with the established thermochemistry for methane-to-ethene conversion, which unambiguously demonstrates that such conversion cannot proceed at thermal energies regardless of the presence of Au_2^+.

Introduction

The typical picture of a catalytic process is that of a thermodynamically favorable, kinetically inhibited reaction made possible by the opening of a lower energy or more efficient pathway through complexation with the catalyst.[1] For instance, the oxidation of CO by O_2 does not proceed at room temperature despite being exothermic by ~3 eV, but occurs readily in the presence of a platinum catalyst, which provides a pathway to efficiently dissociate the dioxygen. A key aspect of any catalytic process is that it cannot alter the thermodynamics of the reactants and the products, only the intermediates that couple them.

Thus, catalyzing a thermodynamically unfavorable process is an uphill battle; however, Lang et al.[2-4] reported and detailed the conversion of methane to ethene at room temperature enabled by Au_2^+. The overall reaction (1),

$$2\ CH_4 \rightarrow C_2H_4 + 2\ H_2 \qquad\qquad \Delta_rH^o_{298} = 2.0883 \pm 0.0016\ \text{eV} \quad (1)^{[5]}$$

is significantly endothermic and endoergic ($\Delta_rG^o_{298} = 1.7542$ eV)[6] such that the calculated equilibrium constant, $K = \exp(-\Delta_rG^o_{298}/RT) \sim 10^{-30}$, implies an immeasurably small forward rate constant at room temperature.[7] Nonetheless, Lang et al. report an overall process corresponding to reaction (1) at temperatures as low as 200 K by introducing methane to mass-selected Au_2^+ in an ion-trap experiment. Through kinetic modeling combined with density functional calculations, the catalytic cycle shown in Scheme 1 was derived. Au_2^+ itself is ancillary to the proposed cycle, reversibly forming $Au_2(CH_4)^+$, which clusters with a second methane to form a $Au_2(CH_4)_2^+$ intermediate. $Au_2(CH_4)_2^+$ overcomes an energetic barrier to undergo a double dehydrogenation, leaving an ethene ligand. The ethene is liberated through ligand exchange with

CH_4, restarting the cycle. This mechanism provides excellent fits to the ion trap data from 200 – 300 K over 2 seconds of reaction time. The reported theoretical reaction coordinate requires surmounting a barrier of approximately 2 eV during the dehydrogenation step,[3] consistent with the overall thermochemistry of reaction (1), but at odds with the observed efficiency at low temperature.

The conversion in reaction (1) has large commercial potential (ethene is a valuable feedstock gas,[8] while the economic value of methane is sufficiently low that large quantities are simply emitted into the atmosphere), and the observation by Lang et al. has received significant interest from the broader chemical community.[9-14] The thermodynamics indicate that the overall cycle cannot occur at thermal energies, but do not speak directly to the formation of intermediate species. Here we aim to more fully decipher the chemistry occurring when CH_4 is in the presence of Au_2^+ in the gas phase. The $Au_2^+ + CH_4$ system is investigated using a selected-ion flow tube (SIFT), which involves pressures about 100 times higher than the ion trap experiments. Separately, a range of relevant reactions of methane with Au_2^+, $Au_2(CH_4)^+$, $Au_2(CH_4)_2^+$, $Au_2(C_2H_4)^+$, and $Au_2(C_2H_4)(CH_4)^+$, including some deuterated analogues, are investigated under single-collision conditions using a guided ion beam tandem mass spectrometer (GIBMS). Additionally, the potential energy surface of the $Au_2^+ + 2\,CH_4$ system is explored again using quantum chemical calculations.

Experimental and Theoretical Methods

Guided Ion Beam Tandem Mass Spectrometer

The GIBMS at the University of Utah used in these studies has been described previously.[15] Briefly, Au_2^+ ions were created in a direct current discharge flow tube (DC/FT) source described in detail elsewhere.[16] Atomic gold cations and neutrals were created when Ar ionized by a DC electric field (1.5 – 1.8 kV) collides with a tantalum cathode to which a gold foil sample is fastened using copper wire. Dimerization and thermalization occur under ~10^5 collisions with the He/Ar carrier gasses in a 9:1 mixture along a 1 m flow tube held at a total

pressure of 0.4 – 0.8 Torr. Methane, ethene, and carbon monoxide adducts of Au_2^+ were produced by introducing CH_4, C_2H_4, or CO ~15 cm downstream of the discharge. Three-body association reactions yielded $Au_2(CH_4)^+$, $Au_2(CH_4)_2^+$, $Au_2(C_2H_4)^+$, and $Au_2(CO)^+$. A species having the mass of $Au_2(28)^+$, isobaric with $Au_2(C_2H_4)^+$ and $Au_2(CO)^+$, could also be formed with only methane and the carrier gases in the source. In all cases, the ions are presumed to have reached thermal equilibrium with the flow tube gases such that their internal temperatures are 300 K. Although the formulae of these species have been designated as adducts, there is always the possibility that the bond connectivity is different than suggested or that the chemical identity is not what is noted above. This can be explored further by the experiments detailed below and by comparison to theory.

In previous experiments, it has been observed that the DC discharge source forms Au^+ in both its ^1S ground and ^3D excited states, with relative probabilities that are influenced by the other gases present.[17, 18,19] With only He and Ar in the flow tube, a very small amount of a state lying over 4 eV above the $^1S_0$ ground state along with ~ 6% of the $^3D_3$ and $^3D_2$ states at 1.865 and 2.187 eV above the ground state are formed. All excited states can be removed by using N_2O as a quenching gas.[19] In contrast, if methane is introduced into the flow tube, the amount of the $^3D_3$ and $^3D_2$ states gradually increases as the methane pressure increases, eventually dominating the Au^+ ions formed (essentially no remaining $^1S_0$ ground state).[19] In the present experiments, methane must be added to the flow tube to form several of the adducts of interest; hence, we also formed these species in the presence of N_2O, which is known to quench the formation of the ^3D excited states. No differences in the results were obtained with and without N_2O present.

The introduction of N_2O in the source potentially complicates the identification of the methane adducts, as oxygen atoms and methane are isobaric. To test whether an Au_2O^+ species or higher order oxide might be contaminating our results, we attempted to generate the Au_2O^+ ion specifically by introducing N_2O, O_2, and water into the source. In no case did the source form an ion corresponding to the mass of Au_2O^+, consistent with results detailed below for the reactions of Au_2^+ with these oxidants.

Once formed, ions were extracted from the source, focused through a magnetic momentum analyzer where the reactant ion was mass selected. These ions were then decelerated to a well-defined kinetic energy and passed into a radiofrequency (rf) octopole ion beam guide[20-22] where the ions were trapped radially. The octopole passes through a static gas cell that contains the neutral reactant gas at pressures of $0.1 - 0.8$ mTorr. Pressures were kept low to ensure that the probability of more than one collision occurring between the reactants was small, and it was verified that the measured cross sections reported below do not vary with neutral reactant pressure. After the collision cell, remaining reactant and product ions drifted to the end of the octopole, were focused through a quadrupole mass filter for mass analysis, and counted using a Daly detector.[23]

Laboratory ion energies (lab) were converted to the center-of-mass frame (CM) using the relationship $E_{CM} = E_{lab} \times m/(m + M)$ where m and M are the masses of the neutral and ionic reactants, respectively. The absolute zero of energy and the full width at half-maximum (FWHM) of the ion beam were determined by using the octopole guide as a retarding potential analyzer.[21] Typical FWHMs of the energy distribution for these experiments were $0.4 - 0.6$ eV (lab). Uncertainties in the absolute energy scale are 0.1 eV (lab). All energies reported below are in the CM frame.

Reaction cross sections were calculated, as described previously,[21] from product ion intensities relative to reactant ion intensities after correcting for product ion intensities with the neutral gas no longer directed to the gas cell. For the purposes of the present work, these absolute kinetic-energy-dependent cross sections, $\sigma(E_{CM})$, were generally converted to rate constants as a function of energy, $k(E_{CM})$, using a procedure outlined in detail elsewhere.[21] Briefly, $k(E_{CM}) = v \times \sigma(E_{CM})$ where $v = (2E_{CM}/\mu)^{1/2}$ is the relative reactant velocity and $\mu = mM/(m + M)$ is the reduced mass of the reactants. As v approaches zero, the rate $k(E_{CM})$ approaches the thermal rate constant at an effective temperature $T' = T \times M/(m + M)$ where T is the temperature of the reactant neutral (305 K). Uncertainties in the measured absolute cross sections and rate constants are estimated to be $\pm 20\%$, with relative uncertainties of $\pm 5\%$.

6

Selected-Ion Flow Tube

The SIFT apparatus at the Air Force Research Laboratory has been described in detail previously.[24]   Briefly, Au_2^+ were created in a DC discharge/flow tube source similar to that described above in the GIBMS experiment. Gold foil (ESPI Metals, 99.95%) was spot-welded around a carbon steel rod and biased at -1 to -3 kV, and discharged to the inside of a 2.5" diameter grounded can drawing ~25 mA through a flow of typically 500 std. cm^3 min^{-1} He and 100 std. cm^3 min^{-1} Ar. After a short distance (2.5 cm), ions were extracted through a 1 mm diameter hole in a rounded nosecone into a higher vacuum region (~10^{-4} Torr) and mass-selected using a quadrupole mass filter. Mass-selected ions were injected via a Venturi inlet into a 7 cm diameter, 1 m long stainless steel flow tube held at a variable pressure (0.3 – 0.6 Torr) of the He buffer gas (Matheson, 99.999%) at a typical flow of 15 std. L min^{-1}. Ions underwent 10^4 – 10^5 collisions with the He buffer gas prior to addition of CH_4 (Airgas, 99.99%) through a stainless steel finger inlet 59 cm prior to the terminus of the flow tube. The wall temperature of the flow tube was variable from 100 K – 700 K via either pulsed liquid nitrogen or resistive heating elements. The center axis of the flow was sampled through a 4 mm aperture in a rounded carbon nosecone and transported to a high vacuum region using a rectilinear (i.e., rods have a square cross-section) quadrupole ion guide. Ions were detected using an orthogonally-accelerated time-of-flight mass spectrometer. Mass discrimination in the rectilinear ion guide is smaller than typical for "normal" round cross-section quadrupole ion guides,[25] such that no discrimination in the relevant mass range (390 – 450 Da) was observed.

Rate constants were determined by monitoring reactant and product ion abundances as a function of CH_4 reactant concentration. Total rate constants for reaction of the primary ion (Au_2^+) were determined from the ion decay by assuming pseudo-first order kinetics. Additional kinetic information and uncertainties were derived by kinetic modeling of the ion abundances as described elsewhere.[26]

Theory

The reaction paths for the $Au_2^+ + 2\ CH_4 \rightarrow Au_2(C_2H_4)^+ + 2\ H_2$ reaction were investigated using density functional theory (DFT). All calculations were performed using the quantum chemistry suite ORCA.[27] Geometry optimizations were carried out with tight convergence criteria ($\Delta W < 10^{-6}$ Hartree) and a tight self-consistent field (SCF) ($\Delta E < 10^{-8}$ Hartree). The stationary points were classified as either transition states (TSs) or intermediates (INTs) on the basis of vibrational frequency calculations at each point. TSs, which are first-order saddle points, were verified to have a single imaginary frequency. To confirm the connectivity of TSs with intermediates, intrinsic reaction coordinate (IRC)[28] calculations were performed.

Although the calculations shown below were done at the B3LYP[29, 30]/def2-TZVPP[31, 32] level of theory, several other different functionals (M06-L, the local version of the Minnesota Functionals from Truhlar and Zhao;[33] and TPSS0, the 25% hybrid exchange version of the meta-generalized gradient approximation of Tao, Perdew, Staroverov, and Scuseria[34, 35]) were tested with different basis sets (LANL2DZ[36, 37] and def2-TZVPP). The results are qualitatively similar.

Results

Observations from SIFT experiments

Data were collected in the SIFT experiment for $Au_2^+ + CH_4$ between $200 - 600$ K at pressures from 0.3 to 0.6 Torr in He buffer gas. Representative data are shown in Figure 1. The dominant products under all SIFT conditions are $Au_2(CH_4)^+$ and $Au_2(CH_4)_2^+$. $Au_2(CH_4)_3^+$ was observed at temperatures of 300 K and below and $Au_2(CH_4)_4^+$ at 200 K. In some experiments, small amounts of *m/z 408* (presumably $Au_2CH_2^+$) and *m/z 422* (possibly $Au_2(C_2H_4)^+$) were observed along with products consistent with clustering to those species (e.g., $Au_2CH_2(CH_4)^+$), whereas at other times under nominally identical conditions, these species were not observed above the noise level of the experiment. The observations of $Au_2CH_2^+$ and $Au_2(C_2H_4)^+$ were always correlated, with either both being present or neither being observed.

The cluster products $Au_2(CH_4)_x^+$ are formed through three-body stabilization of complexes by collision with the buffer gas, i.e., reaction (2).

$$Au_2(CH_4)_n^+ + CH_4 + He \rightleftarrows Au_2(CH_4)_{n+1}^+ + He \tag{2}$$
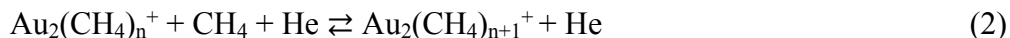
Rate constants derived from kinetic modeling of the data are reported in Table 1. The reverse reaction (2) was found to be negligible for the initial $n = 0$ clustering reaction, but not for the $n = 1 - 3$ reactions at higher temperatures.

Table 1. Rate constants ($\times 10^{-28}$ cm^6 s^{-1}) for reactions (2) derived from the SIFT data. Reverse rate constants ($\times 10^{-15}$ cm^3 s^{-1}) in italics where non-negligible.

Reaction	200 K	250 K	300 K	400 K	500 K
$n = 0^a$	14	7.0	3.1	2	< 2
$n = 1^b$	56	13 / *0.4*	6.5 / *40*	-	-
$n = 2$	observed	observed	observed	-	-
$n = 3$	observed	-	-	-	-

[a] Uncertainty in rate constants ±30%.
[b] Uncertainty in rate constants ±50%.

$Au_2CH_2^+$ could conceivably be formed by reaction (3), analogous to a known reaction for Au^+

$$Au_2^+ + CH_4 \rightarrow Au_2CH_2^+ + H_2 \tag{3}$$

which is calculated to be slightly exothermic. [38] However, calculations show a prohibitive ~0.75 eV activation barrier, see below. Further, GIBMS experiments demonstrate that this reaction does not occur under single collision conditions, see below. Therefore, it appears more likely that the $Au_2CH_2^+$ arises from unquenched excited state Au_2^{+*}. The fraction of $Au_2CH_2^+$ was observed to vary or even be absent when repeating the experiment at different times, presumably a result of variations in source conditions producing varied amounts of Au_2^{+*}. The correlated behavior of $Au_2(C_2H_4)^+$ and $Au_2CH_2^+$ suggests that both arise from the same excited state chemistry. The magnitude of $Au_2(C_2H_4)^+$ observed in the SIFT experiments can be explained by assuming that reaction (4) is occurring.

$$Au_2CH_2^+ + CH_4 \rightarrow Au_2(C_2H_4)^+ + H_2 \tag{4}$$
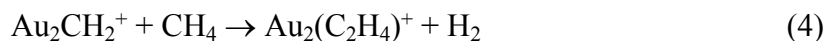
Reaction (4) is calculated to be exothermic; however, the calculated reaction coordinate (see below) indicates a substantial energetic barrier. Alternately, the signal at $Au_2^+(28)$ could be assigned to $Au_2^+(CO)$, arising from an impurity similar to that observed in the GIBMS experiments described below.

The rate constants used in the kinetic modeling of the initial $Au_2^+ + CH_4$ ion trap experiments were not published,[3] making direct comparison of the two experiments more difficult. However, a detailed mechanism and rate constants for $Au_2^+ + CD_4$ were presented in a later publication.[4] To compare the experiments, data were taken using the SIFT apparatus for $Au_2^+ + CD_4$ at room temperature (Figure 2). As for the CH_4 reaction system, the SIFT results primarily produce clustering reactions, analogous to reactions (2), with only minor amounts of $Au_2(C_2D_4)^+$ observed and $Au_2(C_2D_4)(CD_4)^+$ only at the highest $[CD_4]$ conditions. No $Au_2CD_2^+$ was observed.

The previously proposed mechanism to explain the ion trap data is as follows:[4]

$$Au_2^+ + CD_4 \rightleftarrows Au_2(CD_4)^+ \qquad\qquad k_1 = 2.1 \pm 0.5 \times 10^{-13} \text{ cm}^3 \text{ s}^{-1} \quad (5\text{-}1)$$

$$k_{-1} = 0.1 \pm 0.3 \text{ s}^{-1}$$

$$Au_2(CD_4)^+ + CD_4 \rightarrow Au_2(C_2D_4)^+ + 2 D_2 \qquad k_2 = 4.4 \pm 1.2 \times 10^{-12} \text{ cm}^3 \text{ s}^{-1} \quad (5\text{-}2)$$

$$Au_2(C_2D_4)^+ + CD_4 \rightarrow Au_2(C_2D_4)(CD_4)^+ \qquad k_3 = 4.7 \pm 1.2 \times 10^{-12} \text{ cm}^3 \text{ s}^{-1} \quad (5\text{-}3)$$

$$Au_2(C_2D_4)(CD_4)^+ \rightarrow Au_2(CD_4)^+ \qquad\qquad k_4 > 100 \text{ s}^{-1} \qquad\qquad\qquad (5\text{-}4)$$
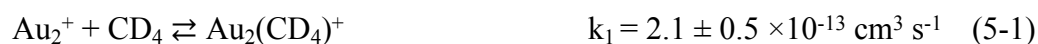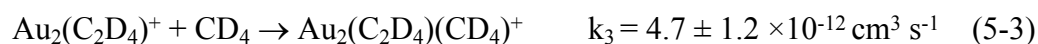
The key reaction in the proposed mechanism is (5-2) yielding an ethene ligand, which if formed allows for the proposed catalytic cycle. Several considerations are necessary to directly compare this mechanism to the SIFT data. First, the SIFT experiments were conducted at 0.35 Torr of He, whereas the ion trap experiments were at 0.008 Torr (95% He) necessitating conversion of the reported two-body constants for clustering reactions to three-body rate constants and including the He buffer gas as a third-body. Over a limited pressure range of 0.3 to 0.6 Torr of He in the SIFT experiment, the $Au_2^+ + CD_4$ clustering reaction rate constants were found to scale linearly with pressure indicating they are in the low pressure regime. Additionally, statistical modeling of the clustering reactions (to be described in detail elsewhere) also shows them to be

in the linear regime at these higher pressures. Conversion of the rate constants appears justifiable, while recognizing that CD_4 accounts for ~6% of collisions in the ion trap and compared to < 0.5% of collisions in the SIFT. CD_4 collisions likely stabilize the complexes more efficiently than do He collisions, and the three-body rate constants used below may be somewhat overstated. Second, $Au_2(CD_4)_2^+$ is not observed in the ion trap experiments at 300 K, but is assumed to be an intermediate in their proposed mechanism. $Au_2(CD_4)_2^+$ is observed in the SIFT experiment and is explicitly represented in the reaction scheme. Third, reaction (5-4) is presented as a unimolecular process and only a lower limit is placed on the rate constant. Here, this reaction is handled in two limiting cases in modeling the SIFT data: 1) as shown in reaction (5-4), the minimum rate constant of 100 s^{-1} is assumed, thereby setting a lower bound; and 2) setting an upper bound by combining reactions (5-3) and (5-4) into a single bimolecular step occurring at the capture rate of 8×10^{-10} cm^3 s^{-1}. The latter case is also modeled assuming a rate constant of 2×10^{-11} cm^3 s^{-1} for the combined reactions (5-3) and (5-4), as reported below from the GIBMS experiment.

In Figure 2, little to no signal is observed corresponding to $Au_2(C_2D_4)^+$ (m/z = 426 Da) or $Au_2(C_2D_4)(CD_4)^+$ (m/z = 446 Da). Small amounts of these masses observed at higher [CD_4] are similar to the noise level of the experiment and should be considered upper limits. The modeled fits assuming the proposed mechanism derived from the ion trap experiment exceed the observed abundance of $Au_2(C_2D_4)^+$ by at least a factor of 5 in the most limiting case (case 1), and by a factor of at least 40 in case 2. Similarly, the modeled fit of $Au_2(C_2D_4)(CD_4)^+$ exceeds the observed abundance by at least a factor of 300 assuming the mechanism that allows for its formation. The SIFT and ion trap data are not compatible, with the former observing ethene only under unusual, transient conditions.

Observations from GIBMS experiments

For the purposes of the present study, the GIBMS results focus on those reactions that can be observed at thermal conditions. Endothermic processes observed are mentioned here but their analysis and resulting thermochemistry will be presented in a forthcoming publication.

Reactions of Au$_2^+$ with methane. In the ion trap studies,[2-4] the only reaction observed between the gold dimer cation and methane is three-body association to form the Au$_2$(CH$_4$)$^+$ adduct. Subsequent spectroscopic studies verify that the adduct is the dominant structure formed but that the insertion species, HAu$_2$CH$_3^+$ is also formed in small amounts.[39] SIFT experiments find that adduct formation is the dominant product observed, with small amounts of Au$_2$CH$_2^+$ also seen in some experiments. Consistent with these observations, the present studies of the reaction of Au$_2^+$ with CH$_4$ and CD$_4$ under single collision conditions (where an adduct cannot be collisionally stabilized) yield no products at thermal energies. In reaction with CD$_4$, both Au$_2$D$^+$ and Au$_2$CD$_3^+$ are formed in processes exhibiting appreciable barriers. The CH$_4$ reactant gives Au$_2$CH$_3^+$ with a similar cross section to that for Au$_2$CD$_3^+$, but that for Au$_2$H$^+$ could not be determined accurately because of mass overlap with the reactant beam. Notably, there is no evidence for the formation of Au$_2$CH$_2^+$ (Au$_2$CD$_2^+$), although these products were looked for carefully. This is consistent with the hypothesis that formation of this species requires an electronically excited Au$_2^+$*.

Reaction of Au$_2^+$(CH$_4$) with methane. In the proposed catalytic cycle, this reaction is the key step, as it leads to formation of ethene. In GIBMS work, the dominant process observed is collision-induced dissociation (CID) to lose a single methane molecule, reaction (6), as shown in Figure 3a.

$$Au_2(CH_4)^+ + CH_4 \; \rightarrow \; Au_2^+ + 2\;CH_4 \tag{6}$$

Reaction (6) must be an endothermic process, consistent with the kinetic energy dependence of the Au$_2^+$ rate constant. Further, the threshold for this CID process is quite low, consistent with an adduct as the precursor.

In addition to this dominant endothermic process, a barrierless exothermic reaction was also observed, consistent with double dehydrogenation and formation of gold dimer cations bound to a species having a mass of 28, reaction (7).

$$Au_2(16)^+ + CH_4 \rightarrow Au_2(28)^+ + 2\ H_2 \tag{7}$$

This reaction is the key process of interest observed in the ion trap studies, the ostensible formation of ethene (*m/z* 28). As determined on multiple occasions, this cross section showed no dependence on the methane reactant pressure, indicating it corresponds to single collision conditions. A product corresponding to loss of a single H_2 molecule was explicitly looked for and never observed (nor was such a product ever observed in the ion trap or SIFT experiments).

Because of its critical importance in the original work, reaction (7) was studied upon multiple occasions. Under conditions similar to those used to obtain the data discussed below for reaction of $Au_2(CH_4)_2^+$, the blue data shown in Figure 3a was obtained. Here, reaction (7) exhibits an energy independent rate constant of $k(7) = 5.3 \pm 2.9 \times 10^{-13}$ cm^3 s^{-1} below 0.5 eV, dropping slightly at higher energies. This experiment was repeated on another day, with identical results for the CID reaction (6), but now $k(7) = 2.2 \pm 0.8 \times 10^{-12}$ cm^3 s^{-1} (red data of Figure 3a), with the rate constant again being pressure independent with the same energy dependence as before. Note that this latter rate constant is comparable to that reported for the analogous perdeuterated reaction (5-2). At a later date, using a new Au foil sample in the source, we discovered that the rate observed for reaction (7) changed with time during a single experimental run. This temporal effect was observed upon several occasions with one example shown in Figure 3b. Data taken immediately after starting the discharge shows the largest thermal rate constant for reaction (7), $k(7) = 5.2 \pm 1.0 \times 10^{-11}$ cm^3 s^{-1} (red data), which drops to $1.6 \pm 0.3 \times 10^{-11}$ cm^3 s^{-1} after 40 minutes (green data), and then to $3.4 \pm 0.7 \times 10^{-12}$ cm^3 s^{-1} after another 40 minutes (blue data), at which point, it stabilized.

At this point, we intended to see whether we could test whether the disparate results for reaction (7) could be attributed to electronically excited species, e.g., $Au_2^+{}^*$, as suggested above. Hence, we added N_2O to the He, Ar, and CH_4 flow gases, as this species is known to quench all

electronically excited states of atomic Au^+.[19] On this day, our first data set yielded very different results for the CID reaction (6) and reaction (7) was much more efficient, $k(7) = 1.0 \pm 0.2 \times 10^{-11}$ cm^3 s^{-1} and declined with energy to about half that value by 0.15 eV. In the next data set, taken approximately 40 minutes after the first was started, the CID cross section had reverted back to that shown in Figure 3a and $k(7)$ dropped to $\sim 2 \pm 0.4 \times 10^{-12}$ cm^3 s^{-1}. The next four data sets (started 40 minutes after the second and extending for the next several hours), taken both with and without N_2O in the source, had identical CID cross sections as Figure 3a and $k(7) = 1.9 \pm 0.7$ $\times 10^{-13}$ cm^3 s^{-1}, with an energy dependence similar to that shown in Figure 3a.

We next discovered that the formation of Au_2^+ was enhanced by the presence of O_2 in the flow tube, so in this series of experiments, O_2 was added to the He, Ar, and CH_4 flow gases. Of course, addition of O_2 could be problematic if it allowed formation of Au_2O^+, isobaric with $Au_2^+(CH_4)$, but as discussed in detail below, in the absence of methane, no Au_2O^+ is formed. Under these conditions, results of the first two data sets were reproducible with an example shown in Figure 3c. Again the CID cross section forming Au_2^+ showed different behavior than Figure 3a, more similar to the first data set of the N_2O sequence above. Here, $k(7)$ was 2.0 ± 0.4 $\times 10^{-11}$ cm^3 s^{-1} at thermal energies, declining to about $0.8 \pm 0.2 \times 10^{-11}$ cm^3 s^{-1} by 0.15 eV. This energy dependence matches that obtained for the first data set in the N_2O sequence. After about 2 hours, the results again began to change, eventually reverting to those identical to Figure 3a.

The fact that the rate constant for reaction (7) can vary over two orders of magnitude depending on source conditions (which are not totally controllable) indicates that a transient species is the component responsible for reaction (7). This could plausibly be an excited electronic state of Au_2^+, which is potentially consistent with our previous observations that electronically excited Au^+ is formed abundantly in our DC discharge source when methane is present and survives thousands of collisions with both atomic and molecular flow gases.[19] However, the survival of an electronically excited *molecular* species under such conditions is certainly unusual and to our knowledge unprecedented. One could imagine that the reactive component is the $HAu_2CH_3^+$ species identified spectroscopically; however, this species does not

have sufficient energy to overcome the intrinsic endothermicity of reaction (1). The other plausible candidate for the reactive species is the oxide, Au_2O^+, although its formation appears to require the presence of both an oxidant and methane. This observation suggests that the oxide is only formed when electronically excited Au^+ is available, similar to the suggestions that reaction (3) requires a $Au_2^+{}^*$ reactant.

The temporal dependence of the results for reactions (6) and (7) is more mysterious, although we have reproduced this behavior on several occasions. One possibility is that the components needed to form the reactive $Au_2^+(16)$ species (whether it is an oxide or electronically excited methane complex) are available either on the surface of the newly installed gold foil, which may also depend on the condition of the foil itself, or in the residual gases available in the vacuum chamber after pumping down. Operation of the source eventually removes these components and the reactive species decreases to a background level. Indeed, studies performed where the source was allowed to pump for a day after installing the gold foil yielded no enhanced formation of $Au_2(28)^+$ in reaction (7). At this point, we considered whether introducing an appropriate contaminant into the source and maintaining its presence would allow a stable yield of the reactive species to be produced. This was attempted by introduction of either O_2 or H_2O into the source along with methane, but no stable enhanced yield of the $Au_2(28)^+$ product was observed. Another possibility is that the reactive component is dependent on the temperature of the source, which gradually increases over time (even though water cooled) because of the very energetic discharge conditions. Another possibility is that the formation of appreciable amounts of the reactive component depend on the condition of the foil itself (which varied appreciably in various experiments as new foil was ordered multiple times over the course of the months during which these experiments were conducted).

Reactions of $Au_2^+(CH_4)_2$ with methane. As for the single methane adduct, the dominant process observed when the double adduct interacts with methane under single collision conditions is the CID process (8).

$$Au_2(CH_4)_2^+ + CH_4 \rightarrow Au_2(CH_4)^+ + 2\ CH_4 \qquad (8)$$

This rate constatnt is shown in Figure 4. These reactants also can lose a second methane ligand at higher collision energies, in a process that exhibits some dependence on the methane reactant pressure, as is common for secondary CID processes.[40, 41]

In addition to these endothermic processes, an inefficient barrierless exothermic reaction was also observed, consistent with double dehydrogenation and formation of gold dimer cations bound to a species having a mass of 28, reaction (9).

$$Au_2^+(CH_4)_2 + CH_4 \ \rightarrow \ Au_2^+(28)(CH_4) + 2\ H_2 \tag{9}$$
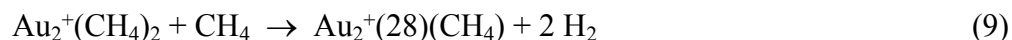
Reaction (9) was examined at two pressures (differing by a factor of two) on the same day, yielding rate constants in good agreement with one another. Thus, the rate constant shown corresponds to single collision conditions. Again, a product corresponding to loss of a single H_2 molecule was explicitly looked for and never observed. At thermal energies, $k(9) = 1.2 \pm 0.2 \times 10^{-12}$ cm^3 s^{-1}. As can be seen in Figure 4 (which shows the average of the two data sets), this rate constant may decline slightly as the energy increases, falling to about half that value by an energy of 0.4 eV and disappearing into the noise at higher energies.

Reactions of Au$_2^+$(C$_2$H$_4$) with methane. In this study, the reactant ion was generated by introducing ethene into the source, thereby forming an authentic sample of $Au_2^+(C_2H_4)$. Two processes were observed in this reaction, simple CID and ligand exchange, reactions (10) and (11), respectively, as shown in Figure 5.

$$Au_2(C_2H_4)^+ + CH_4 \quad \rightarrow \ Au_2^+ + C_2H_4 + CH_4 \tag{10}$$
$$\rightarrow \ Au_2^+(CH_4) + \ C_2H_4 \tag{11}$$
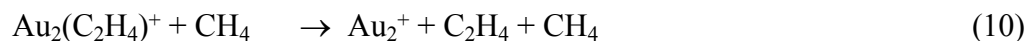
Clearly, CID is efficient but endothermic, whereas the exchange reaction is barrierless, exothermic, and relatively inefficient. The rate constant for the latter process falls rapidly with energy, primarily a consequence of competition with the CID process. At thermal energies, the rate constant is $k(11) = 2.0 \pm 0.4 \times 10^{-11}$ cm^3 s^{-1}. The observation of reaction (11) as exothermic indicates that methane binds more tightly to the gold dimer cation than ethene, certainly an unusual result, but one consistent with the final step of the "catalytic cycle" reported by Lang et al.,[3] the analogues of reactions (5-3) and (5-4).

Potential oxide formation. As mentioned above, there was concern that the methane adducts might be contaminated by an oxide. Indeed, the exothermic reaction (12) could potentially explain the original ion trap results as this exothermic reaction actually can be catalyzed by Au_2^+.

$$O + CH_4 \rightarrow CO + 2\,H_2 \qquad \Delta_rH°_{298} = -2.9522 \pm 0.0037 \text{ eV} \qquad (12)$$

This possibility was investigated by several independent routes. As noted above, N_2O, O_2, and H_2O were introduced into the flow tube, but no formation of Au_2O^+ was observed. To verify that these oxidants should not yield Au_2O^+, we examined the reactions of Au_2^+ with all three gases in the reaction cell. No products were observed up to 2.6 eV in the reactions with O_2 and D_2O. Because the intensity of the Au_2^+ reactant beam was fairly small, these results put upper limits of about 0.1 and 0.2×10^{-16} cm^2, respectively, on the cross sections for any products. In the case of N_2O (which has a much weaker oxide bond compared to O_2 and D_2O), formation of Au_2O^+ was observed with an apparent threshold near 2 eV and a maximum cross section of 0.5×10^{-16} cm^2 at 7 eV. These results confirm that formation of Au_2O^+ should not occur with readily accessible oxidants at thermal energies with ground state Au_2^+ reactants.

Although these results are seemingly definitive, it can still be imagined that oxygen or water adsorbed on the gold foil, which could vary depending on the condition of the foil itself, or in the residual gases remaining from venting the ion source might allow for formation of small amounts of Au_2O^+. Further, it can be noted that these oxidation experiments were conducted in the *absence* of methane in the flow tube. Thus, it remains possible that electronically excited states of Au^+ (formed when methane is present) allow the formation of Au_2O^+ with trace oxygenating reagents. Of course, under these conditions, $Au_2^+(CH_4)$ should also be produced, such that the identity of the ion that is present in abundance cannot be determined with certainty. Experiments to confirm or refute these various possibilities are not straightforward, but two possibilities were explored as detailed next.

Reactions of $Au_2^+(CH_4)$ with deuterated methane. In these experiments, the reactant ion was generated with methane (along with the He/Ar flow gasses) in the source, but no oxidant

was introduced. As shown in Figure 6, the dominant process observed is an exothermic ligand exchange reaction (13).

$$Au_2(CH_4)^+ + CD_4 \rightarrow Au_2(CD_4)^+ + CH_4 \tag{13}$$

This process has a rate constant at thermal energies of $k(13) = 3.6 \pm 0.7 \times 10^{-10}$ cm^3 s^{-1}, such that the efficiency compared to the collision rate constant[42] is 40%, consistent with expectations for two ligands having essentially equal binding energies. This rate becomes less efficient with increasing energy, dropping to 13% by 0.5 eV and 7% above 1 eV. This behavior is consistent with formation of a short-lived $Au_2(CH_4)(CD_4)^+$ adduct. The endothermic CID process (14) was also observed and has an identical magnitude and energy dependence as that observed for reaction (6).

$$Au_2(CH_4)^+ + CD_4 \rightarrow Au_2^+ + CH_4 + CD_4 \tag{14}$$

Finally, reaction (15a), the analogue of reaction (7), was also observed and has an identical magnitude and energy dependence as that shown in Figure 3a (blue data).

$$Au_2(CH_4)^+ + CD_4 \rightarrow Au_2(28)^+ + 2\ D_2 \tag{15a}$$
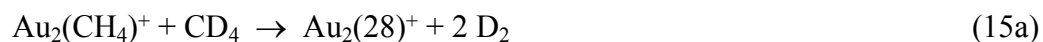
We also looked for $Au_2(29)^+$, $Au_2(30)^+$, $Au_2(31)^+$, and $Au_2(32)^+$, which would correspond to the isotopomers of $Au_2(C_2H_4)^+$, but these products were never observed. Indeed, intensity at $Au_2(30)^+$ was specifically collected in several data sets for this reaction, but no hint of this product was observed. Statistically, the dehydrogenation of two methane molecules would preferentially yield the mixed $C_2H_2D_2$ (*m/z 30*) product along with other mixed isotopomers. In any event, it is highly unlikely that double dehydrogenation of $Au_2(CH_4)(CD_4)^+$ would yield exclusive loss of 2 D_2, as was observed here. Of course, this observation is easily explained if reaction (15a) actually corresponds to reaction (15b).

$$Au_2O^+ + CD_4 \rightarrow Au_2(CO)^+ + 2\ D_2 \tag{15b}$$

Note that the amount of Au_2O^+ may easily be a minor component of the $Au_2(16)^+$ reactant beam, which would explain the large variability in the rate constant for reaction (7), Figure 3, and the strong dependence on source conditions. Because of the large exothermicity of reaction (12), this

also explains why loss of a single H_2 (or D_2) molecule is never observed as dehydrogenation of formaldehyde is an isoenergetic process.

Given these results, one imagines that reaction (9) is also associated with a low-level oxide contaminant, $Au_2O(CH_4)^+$, isobaric with $Au_2(CH_4)_2^+$, which then reacts to yield $Au_2(CO)(CH_4)^+$. Because of the low-level signals involved, this hypothesis was not tested using reaction with CD_4.

We also considered examining the reaction of $Au_2(CD_4)^+$ formed in the source, as this reactant would no longer be isobaric with Au_2O^+. Unfortunately, the amount of CD_4 required to generate a usable signal of $Au_2(CD_4)^+$ was prohibitive.

Collision-induced dissociation of Au$_2$(28)$^+$. To test the identity of the $Au_2(28)^+$ product formed in reaction (7), we examined the CID of this species with Xe. Here, the $Au_2(28)^+$ ion was generated in the source by the introduction of methane (with no oxidants), which should form the same species as that generated in reaction (7). Notably, the intensity of this species was quite small (consistent with the inefficient reaction to form it as reported in Figure 3a and in the SIFT experiments). To test its identity, $Au_2(C_2H_4)^+$ and $Au_2(CO)^+$ were also generated by introducing ethene and carbon monoxide, respectively, into the source. The results of these CID processes are shown in Figure 7. It can be seen that the only process observed in all three cases is the loss of the ligand yielding Au_2^+, reaction (16).

$$Au_2(L)^+ + Xe \rightarrow Au_2^+ + L + Xe \qquad (16)$$

Clearly, the ethene is less strongly bound to Au_2^+ than the CO by an appreciable amount, such that the rate constant for L = C_2H_4 is much larger than that for L = CO at low energies, but comparable at higher collision energies. When methane is introduced into the source to generate $Au_2^+(28)$, its CID rate constant matches the energy dependence of the L = CO sample with a magnitude that is nearly the same (factor of two smaller). Although there is some ambiguity because of the noise in this spectrum (a consequence of the very low reactant signal level), the combination of its magnitude and energy dependence clearly indicates that $Au_2^+(28)$ formed in

the source by reactions with methane is actually the carbon monoxide adduct with no discernible

contribution from the ethene adduct.

Theoretical Results

The reaction paths between the $Au_2^+ + 2\ CH_4$ reactants and $Au_2(C_2H_4)^+ + 2\ H_2$ products

have been exhaustively searched using DFT. Instead of allowing both methane molecules to bind

with Au_2^+ as in Ref. 3, we explored an alternative route by binding one methane at a time. The

results are shown in Figure 8, in which various intermediates and transition states are included.

The calculated reaction energy for reaction (1), with zero-point energy corrections, is 2.03 eV,

which is in good agreement with the experimental value (2.0883 ± 0.0016 eV). Comparing to the

earlier proposed pathway of Lang et al.[3] (Table 2), the pathway provided here has similar high-

energy barriers. Specifically, the steps that extract the hydrogen from its respective starting CH_4

each require between $1 - 2$ eV of energy both here and in Ref. 3.

Table 2. Calculated energies (eV) of various stationary points along the reaction path.

Species	Energy (eV)	
	This work	Lang et al.[a]
Reactants	0.00	0.0
INT1	-1.37	-0.9 (INTA)
TS1	-0.57	-
TS1'	0.86	-
Int2	-1.10	-
TS2	0.94	-
Int3	0.66	-
TS3	1.10	-
INT4	-0.67	-
$Au_2CH_2^+ + H_2 + CH_4$	-0.13	-

INT5	-0.72	-
TS4	0.75	-
INT6	-0.75	-
TS5	-0.11	-
INT7	-0.84	-0.2 (INTO)
TS6	0.07	-0.5 (TSP)
INT8	-0.67	-0.1 (INTQ)
TS7	0.00	-
INT9	-0.81	-
INT10	-0.58	0.2 (INTS)
$Au_2^+ + C_2H_4 + 2H_2$	2.03	-

[a]Estimated from Figure 2 of Ref. 3.

In this work, the complexation of Au_2^+ with the first methane (INT1) features a strong (1.37 eV) interaction between the cationic metal dimer and methane. Both the dimer and CH_4 experience minor distortions from their respective equilibrium geometries. From this intermediate, both concerted (TS1') and stepwise (TS1) dehydrogenation pathways were explored. The stepwise pathway has a transition state (TS1) with one hydrogen moving around the first gold atom, leading to a H shared by the Au dimer with a $Au-CH_3$ bond (INT2). The extraction of another H from the CH_3 moiety requires a high energy transition state (TS2), 2.31 eV above INT1, leading to two Au-bound hydrogen atoms and a CH_2 moiety between the two Au atoms (INT3). This is followed by the migration of an H from one Au to another (TS3), resulting in the formation of an H-H bond on one side of the Au dimer (INT4). H_2 can then dissociate from INT4 easily as it is bound by only 0.54 eV. Alternatively, H_2 can be eliminated via a concerted transition state (TS1'), which has a higher energy than TS1, but lower than TS2 and TS3. Both pathways require the system to overcome barriers that are more than 2 eV above INT1 (and >0.86 eV above reactants).

The $Au_2CH_2^+$ species is then approached by a second methane, forming the complex INT5. A C-C bond is formed between CH_2 and CH_4 via TS4 leading to INT6. This is followed by sequential extraction of H via TS5 and TS6, eventually leading to INT8, in which there is a terminal and bridging H atom ligand. This is followed by the migration of an H from one Au to another, forming an H-H bond with the H_2 bound to one Au atom and the C_2H_4 bound to the other Au atom (INT9). This allows another H_2 to form, which costs only 0.23 eV, leaving behind the $Au_2(C_2H_4)^+$ product, INT10. Loss of the ethene ligand from INT10 to complete the catalytic cycle requires 2.61 eV.

In their theoretical exploration of $Au_2^+ + 2\ CH_4$ reaction, Lang et al.[3] take a different approach than that shown in Figure 8. They start with the bis adduct, $Au_2(CH_4)_2^+$ (INTB in Figure 2 of ref. 3), which lies about 1.5 eV below reactants. Sequential activation of both methanes ensues with a rate-limiting step (TSI about 0.3 eV above reactants) yielding $CH_3Au_2CH_3^+$ (INTK) where a single H_2 molecule has been eliminated. Because INTK lies about 0.3 eV below reactants and subsequent steps are much more energetic, this PES suggests that the $Au_2(CH_3)_2^+$ (single dehydrogenation) product probably should have been observed if this mechanism were operative. From INTK, another CH bond is activated (TSL requires 1.1 eV more energy than the reactants) followed by coupling of the CH_2 and CH_3 ligands over TSN (~1.8 eV above reactants). This forms INTO which has a bridging H atom and an ethyl ligand attached to one gold atom. A series of steps activates another CH bond and couples the two hydrogen atoms (with TSP and TSR lying 0.5 and 0.8 eV more than reactants) to form $Au_2(C_2H_4)^+ + H_2$ (INTS), which can attach another methane (INTT) and then lose the ethene ligand at a cost of about 2 eV. Thus, the calculated PES is roughly consistent with the thermochemistry in reaction (1) and contains barriers of ~1.8 eV (TSN) or 1.75 eV (INTU, formation of the $Au_2(CH_4)^+ + C_2H_4 + 2\ H_2$ products). Notably, the PES shown in Figure 8 has lower energy barriers than those found by Lang et al.[3] and eventually is limited by the formation of the final products, $Au_2^+ + C_2H_4 + 2\ H_2$. In either case, the present calculations do not suggest there is anything incorrect about the previously calculated reaction potential energy surface.

Discussion

The well-established thermodynamics of reaction (1) preclude methane-to-ethene conversion at or below room temperature at typical pressure conditions. The thermodynamics of the overall process do not speak directly to the possibility of intermediates formed in the presence of Au_2^+. Neither do they preclude reaction (1) proceeding at elevated temperatures; reaction (1) is entropically favorable because 3 moles of gas are produced from every 2 moles of reactants, such that a measurable amount of conversion becomes possible at $\sim$ 1000 K (similar to methane steam reforming ($CH_4 + H_2O$) and dry reforming ($CH_4 + CO_2$) reactions, which are similarly endothermic).

The GIBMS results (Figure 5) indicate an exothermic ligand exchange, reaction (11), implying that CH_4 is more strongly bound to Au_2^+ than is C_2H_4. The calculations show that the $Au_2(C_2H_4)^+$ structure with an ethene bound "side-on" is the global minimum with a 2.61 eV bond energy (INT10). In addition, two other isomers were located: an ethene bound "end-on" lying 0.5 eV higher in energy, and two CH_2 groups each bridging the Au atoms, which lies $\sim$2 eV higher in energy. The former two possible structures are calculated to have larger bond energies than the Au_2^+-CH_4, calculated as 1.37 eV. This discrepancy of the calculated bond energies with experiment is large, but not out of line for DFT calculations.[43] We note that the ionization energy of $Au_2(C_2H_4)^+$ calculated using the CAM-B3LYP functional is in good agreement with an experimental value.[44] Importantly, the experimental observation that the C_2H_4 is bound less strongly than the CH_4 places a lower limit on the endothermicity of $Au_2(CH_4)^+ + CH_4 \rightarrow Au_2(C_2H_4)^+ + 2\ H_2$ being equal to the endothermicity of reaction (1). It follows that the thermodynamic argument can be extended to preclude the formation of $Au_2(C_2H_4)^+$ from ground state reactants in the proposed catalytic cycle. The proposed reaction sequence (5-1) – (5-4) and its perprotio analogues in Scheme 1 may only proceed as far as reaction (2), clustering to form $Au_2(CH_4)_2^+$, consistent with the SIFT results, which deviate from the proposed catalytic cycle at that point. This conclusion is also consistent with the calculated reaction coordinates (Figure 8

and Figure 2 of Ref. 3), showing prohibitive barriers for all channels other than methane association.

Although $Au_2(28)^+$ is observed to be formed from $Au_2(16)^+ + CH_4$ in the GIBMS experiments, the evidence presented above shows this reaction probably corresponds to $Au_2(CO)^+$ being formed from Au_2O^+. Could this isobaric scenario also explain the observations in the ion trap data? In short, this seems unlikely. $Au_2(28)^+$ is a dominant product in the ion trap experiments, reaching up to 60% of the initial Au_2^+ abundance, inconsistent with a mechanism that requires formation of Au_2O^+ from reaction with trace species. Ion trap experiments were also conducted with CD_4 producing both $Au_2(20)^+$ (i.e., $Au_2(CD_4)^+$) and $Au_2(32)^+$ (i.e., $Au_2(C_2D_4)^+$) peaks with no indication of $Au_2(16)^+$ or $Au_2(28)^+$ peaks.[4] Experiments using Pd_2^+ show analogous results indicating $Pd_2(C_2D_4)^+$ formation from CD_4, although without indication of the thermodynamically prohibited catalytic cycle.[4] The differences in the experimental results cannot be simply explained by differences in the experimental conditions. The ion trap and the SIFT experiments differ in two primary ways. First, the SIFT experiment is at higher pressure, on the order of 0.5 Torr, >99% of which is He buffer gas, while the ion trap is at ~10 mTorr, about 95% of which is He buffer gas and the remnant reactant CH_4. We note that the concentrations of CH_4 are similar in the two experiments, $\sim 3 \times 10^{13}$ cm^{-3}. Second, the ion trap experiment has a reaction time on the order of seconds, while the SIFT experiment is on the order of ms. The extent of reaction for any three-body process (e.g., reaction (2)) will be about 20× greater in the ion trap experiment (a factor of 1/50× in the pressure offset by a factor of 1000× in reaction time), while the extent of reaction for any bimolecular process with CH_4 will be about 1000× greater in the ion trap. This suggests that the much smaller amount of $Au_2^+(C_2H_4)$ observed in the SIFT experiment could be because this product stems from an initial bimolecular process, as opposed to a reaction chain initiated by the clustering reactions (2). Our initial attempt to reconcile the experimental results was to assume that the exothermic reaction (3) to yield $Au_2CH_2^+$ was in competition with methane clustering (reaction (2), n = 0) and led ultimately to $Au_2(C_2H_4)^+$. We note that assuming this

bimolecular mechanism, excellent fits to the kinetics data for both the ion trap and SIFT experiments at multiple temperatures and pressures were achieved. Although a good fit to kinetics data is necessary for a particular mechanism to be considered correct, it is insufficient alone as proof of correctness. Therefore, we were disabused of this notion by 1) noting that the $Au_2CH_2^+$ peak appeared inconsistently in further SIFT experiments, suggesting that it resulted from reaction with excited state Au_2^{+*} dependent on source conditions, 2) the calculation of a reaction coordinate (Figure 7) showing an ~0.8 eV barrier to $Au_2CH_2^+$ formation, and 3) GIBMS results showing no $Au_2CH_2^+$ formation in the reaction of ground state Au_2^+ with CH_4.

The SIFT and GIBMS results are consistent with one another, with the calculated reaction coordinates, and with the fundamental thermodynamics, but inconsistent with the ion trap results. We are unable to explain the ion trap results, but will suggest that if the observed species are $Au_2(C_2H_4)^+$ and $Au_2(C_2D_4)^+$, they must arise from a non-thermal component. The first electronically excited state of Au_2^+ having a different spin ($^4\Sigma_g^-$) than the $^2\Sigma_g^+$ ground state, presumably that observed at times in the SIFT experiment, has sufficient energy (2.6 – 3.1 eV) to drive the process.[45] However, it is unusual for a diatomic species such as Au_2^{+*} to retain a non-thermal energy distribution for a sufficient time to react under the pressure conditions of the SIFT or ion trap experiments, and would be entirely unexpected for a polyatomic species such as $Au_2(CH_4)^{+*}$ to do so.

Despite the evidence being strong against the ion trap results showing methane-to-ethene formation at room temperature and below, the results should not be disregarded. Unlike the trace $Au_2^+(28)$ signal observed in the GIBMS experiments arising from $Au_2^+(CO)$, the ion trap experiments plausibly form ethene, but this process *must* have an energy source in order to overcome the endothermicity of reaction (1). Practical methods for this conversion would, much like steam-reforming reactions, require high temperatures, but the ion trap results could point to catalysts that are advantageous under those conditions. The unusual feature of Au_2^+ binding ethene less strongly than methane could be beneficial in forming ethene catalytically. The primary benefit of gas-phase studies of catalytically active sites is the ability to derive detailed

mechanistic information enabled by the absence of confounding factors inherent to bulk systems. Further efforts to detail the reactions and mechanisms occurring in the ion trap experiments are warranted.

Conclusions

Literature reports of low-temperature catalytic methane-to-ethene conversion in the presence Au_2^+ run counter to well-established thermodynamics. The chemistry was re-investigated at higher pressures using a selected-ion flow tube (SIFT) apparatus, under single-collision conditions using a guided-ion beam tandem mass spectrometer (GIBMS), and through density functional calculations. The abundance of a key intermediate $Au_2(C_2H_4)^+$ in the SIFT experiment is at least a factor of 5 below that implied by the proposed catalytic cycle, and the small amount observed at times is consistent with arising from electronically excited Au_2^{+*}. $Au_2(28)^+$ observed in the GIBMS experiment is shown to be $Au_2(CO)^+$ arising from transient trace species. The SIFT, GIBMS, and DFT results (as well as the calculations of ref. 3) are all consistent with no chemistry of Au_2^+ other than methane-association occurring at or below room temperature, in accord with the thermodynamics. The results do not provide a clear explanation for the observation of $Au_2(C_2H_4)^+$ in previous ion trap experiments, but suggest that this species arises from non-thermal species, as demanded by the thermodynamics.

References

1.   M. E. Davis and R. J. Davis, in *Fundamentals of Chemical Reaction Engineering*, McGraw Hill, New York, NY, 2003, pp. 133-183.
2.   S. M. Lang, T. M. Bernhardt, R. N. Barnett and U. Landman, *J. Phys. Chem. C*, 2011, **115**, 6788-6795.
3.   S. M. Lang, T. M. Bernhardt, R. N. Barnett and U. Landman, *Angew. Chem. Int. Ed.*, 2010, **49**, 980-983.
4.   S. M. Lang, A. Frank and T. M. Bernhardt, *Catal. Sci. Technol.*, 2013, **3**, 2926-2933.
5.   B. Ruscic and D. H. Bross, *Active Thermochemical Tables (ATcT) based on ver. 1.122 of the Thermochemical Network (2016); available at ATcT.anl.gov*, Accessed January 29, 2019.
6.   M. W. Chase Jr., C. A. Davies, J. R. Downey Jr., D. J. Frurip, R. A. McDonald and A. N. Syverud, *JANAF Thermochemical Tables*, J. Phys. Chem. Ref. Data, 1985.
7.   The maximum forward rate constant k1,max may be determined from the equilibrium constant K, calculated from well-established thermochemical values:

$\Delta_r G^{o298} = \Delta_r H^{o298} - T\Delta_r S^{o298} = 169.25$ kJ mol^{-1}

$K_{298} = \exp(-\Delta_r G^{o298}/k_B T) = 1.67 \times 10^{-30}$

The equilibrium constant is also related to the ratio of the forward and reverse rate constants, with a correction to standard pressure to account for the increase from 2 to 3 moles of gas per reaction:

$K_{298} = k_1(\text{cm}^3\text{ s}^{-1}) / (k_{-1}(\text{cm}^6\text{ s}^{-1}) * 2.4 \times 10^{19}\text{ cm}^{-3})$ where $2.4 \times 10^{19}\text{ cm}^{-3} = 1$ bar converts to standard pressure

$k_1(\text{cm}^3\text{ s}^{-1}) = K_{298} * k_{-1}(\text{cm}^6\text{ s}^{-1}) * 2.4 \times 10^{19}\text{ cm}^{-3}$

A maximum reverse rate constant k$_{-1}$,max is estimated by the capture rate constant for each of the two collisions with CH$_4$ ($\sim 10^{-9}$ cm^3 s^{-1}) and the lifetime of the intermediate complex, t$_{complex}$.

$k_{-1,max}(\text{cm}^6\text{ s}^{-1}) = 10^{-9}(\text{cm}^3\text{ s}^{-1}) * 10^{-9}(\text{cm}^3\text{ s}^{-1}) * t_{complex}(\text{s})$

This leads to an estimate for the maximum forward rate constant as a function of complex lifetime.

$k_{1,max}(\text{cm}^3\text{ s}^{-1}) = 4 \times 10^{-29} * t_{complex}(\text{s})$

t$_{complex}$ of Au$_2^+$(CH$_4$)$_2$ is estimated using statistical unimolecular theory to be on the order of 10^{-8} s, implying a maximum forward rate constant ~ 10 to 15 orders of magnitude too small to convert any CH$_4$ to C$_2$H$_4$ under the conditions of the ion trap experiment.
8.   H. A. Wittcoff, B. G. Reuben and J. S. Plotkin, in *Industrial Organic Chemicals*, John Wiley & Sons, Inc., 3rd ed., 2013, pp. 139-209.
9.   D. Schroeder, *Angew. Chem. Int. Ed.*, 2010, **49**, 850-851.
10.   Y. Li and G. A. Somorjai, *Nano Lett.*, 2010, **10**, 2289-2295.
11.   H. Schwarz, *Angew. Chem. Int. Ed.*, 2011, **50**, 10096-10115.
12.   A. W. Castleman, Jr., *Catal. Lett.*, 2011, **141**, 1243-1253.
13.   T. Takei, T. Akita, I. Nakamura, T. Fujitani, M. Okumura, K. Okazaki, J. H. Huang, T. Ishida and M. Haruta, in *Advances in Catalysis, Vol 55*, eds. B. C. Gates and F. C. Jentoft, 2012, vol. 55, pp. 1-126.
14.   S. Wannakao, C. Warakulwit, K. Kongpatpanich, M. Probst and J. Limtrakul, *ACS Catalysis*, 2012, **2**, 986-992.
15.   S. K. Loh, D. A. Hales, L. Lian and P. B. Armentrout, *J. Chem. Phys.*, 1989, **90**, 5466-5485.
16.   R. H. Schultz and P. B. Armentrout, *Int. J. Mass Spectrom. Ion Processes*, 1991, **107**, 29-48.
17.   F. X. Li and P. B. Armentrout, *J. Chem. Phys.*, 2006, **125**, 133114.

18.   F. X. Li, C. S. Hinton, M. Citir, F. Y. Liu and P. B. Armentrout, *J. Chem. Phys.*, 2011, **134**, 024310.
19.   F.-X. Li, K. Gorham and P. B. Armentrout, *J. Phys. Chem. A*, 2010, **114**, 11043–11052
20.   D. Gerlich, *Adv. Chem. Phys.*, 1992, **82**, 1-176.
21.   K. M. Ervin and P. B. Armentrout, *J. Chem. Phys.*, 1985, **83**, 166-189.
22.   P. B. Armentrout, *Int. J. Mass Spectrom.*, 2000, **200**, 219-241.
23.   N. R. Daly, *Rev. Sci. Instrum.*, 1960, **31**, 264-267.
24.   A. A. Viggiano, R. A. Morris, F. Dale, J. F. Paulson, K. Giles, D. Smith and T. Su, *J. Chem. Phys.*, 1990, **93**, 1149-1157.
25.   C. R. Taormina, E. Nicolette, T. Novak and R. E. Pedder, *56th Meeting of the American Society of Mass Spectrometry*, 2008, https://ardaratech.com/downloads/technical-notes/10-tn-3007-practical-quadrupole-theory-ion-guides/file accessed Oct , 2018.
26.   N. S. Shuman, T. M. Miller, A. A. Viggiano and J. Troe, *Adv. Atom. Mol. Opt. Phys.*, 2012, **61**, 209-294.
27.   F. Neese, *WIREs: Comput. Mol. Sci.*, 2012, **2**, 73-78.
28.   C. Gonzalez and H. B. Schlegel, *J. Chem. Phys.*, 1989, **90**, 2154-2161.
29.   A. D. Becke, *J. Chem. Phys.*, 1993, **98**, 5648-5652.
30.   C. Lee, W. Yang and R. G. Parr, *Phys. Rev. B*, 1988, **37**, 785-789.
31.   F. Weigend and R. Ahlrichs, *Phys. Chem. Chem. Phys*, 2005, **7**, 3297.
32.   F. Weigend, *Phys. Chem. Chem. Phys.*, 2006, **8**, 1057-1065.
33.   Y. Wang, X. Jin, H. S. Yu, D. G. Truhlar and X. He, *Proc. Natl. Acad. Sci. U. S. A.*, 2017, **114**, 8487-8492.
34.   J. M. Tao, J. P. Perdew, V. N. Staroverov and G. E. Scuseria, *Phys. Rev. Lett.*, 2003, **91**, 146401.
35.   V. N. Staroverov, G. E. Scuseria, J. M. Tao and J. P. Perdew, *J. Chem. Phys.*, 2003, **119**, 12129-12137.
36.   P. J. Hay and W. R. Wadt, *J. Chem. Phys*, 1985, **82**, 270.
37.   T. H. Dunning Jr and P. J. Hay, in *Modern Theoretical Chemistry*, ed. H. F. Schaefer III, Plenum, New York, 1977, vol. 3, pp. 1-28.
38.   S. Zhou, J. Li, X. N. Wu, M. Schlangen and H. Schwarz, *Angew. Chem. Int. Ed.*, 2016, **55**, 441-444.
39.   S. M. Lang, T. M. Bernhardt, V. Chernyy, J. M. Bakker, R. N. Barnett and U. Landman, *Angew. Chem. Int. Ed.*, 2017, **56**, 13406-13410.
40.   D. A. Hales, L. Lian and P. B. Armentrout, *Int. J. Mass Spectrom. Ion Processes*, 1990, **102**, 269-301.
41.   C. Iceman and P. B. Armentrout, *Int. J. Mass Spectrom.*, 2003, **222**, 329-349.
42.   G. Gioumousis and D. P. Stevenson, *J. Chem. Phys.*, 1958, **29**, 294-299.
43.   E. R. Johnson and A. D. Becke, *J. Chem. Phys*, 2017, **146**, 211105.
44.   R. B. Metz, G. Altinay, O. Kostko and M. Ahmed, *J. Phys. Chem. A*, 2019, **in press**, DOI: 10.1021/acs.jpca.1028b12560.
45.   C. J. Owen, N. R. Keyes, H. Guo and P. B. Armentrout, *J. Chem. Phys.*, 2019, **submitted**.
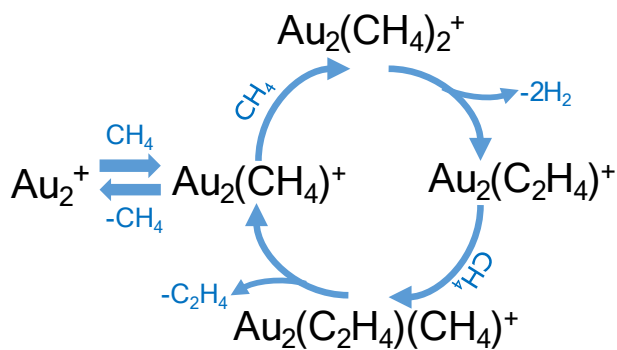
Scheme 1. Proposed catalytic cycle inferred from ion-trap experiments in Refs. [2, 3].
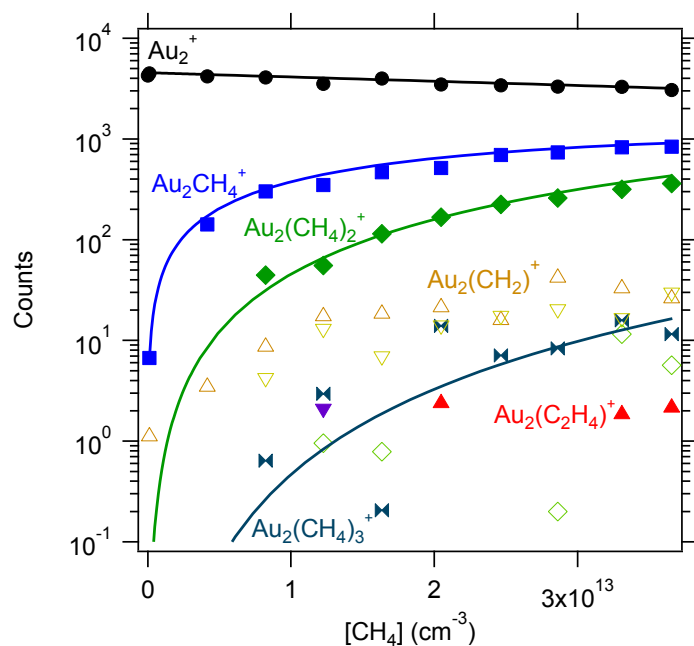
Figure 1. Ion counts obtained using the SIFT (points) for $Au_2^+ + CH_4$ at 300 K, 0.31 Torr of He, and 2.3 ms reaction time as a function of $[CH_4]$ with kinetic modeling fits (solid lines) assuming only the clustering reactions (2) occur. Additional species observed (see text) are shown: $Au_2(CH_2)(CH_4)_n^+$: n=0 (open up triangles), n=1 (open down triangles), n=2 (open diamonds), and $Au_2(C_2H_4)(CH_4)_n^+$: n = 0 (solid up triangles) and n = 1 (solid down triangle).
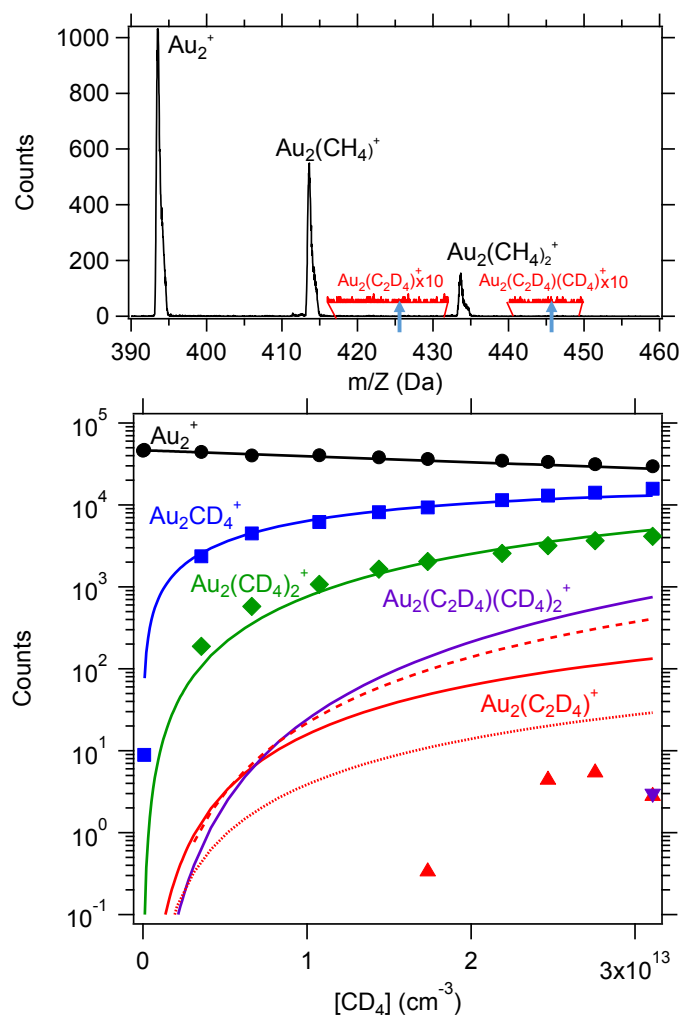
Figure 2. (Lower panel) Ion counts obtained using the SIFT (points) for $Au_2^+ + CD_4$ at 300 K, 0.35 Torr of He, and 2.3 ms reaction time as a function of $[CD_4]$ with kinetic modeling fits (dotted line, case 1; solid lines, case 2) under the limiting cases described in the text; dashed line, as case 2) but assuming the rate constant for reaction 11 reported from the GIBMS results. Models for Au_2^+, $Au_2(CD_4)^+$, and $Au_2(CD_4)_2^+$ are unchanged between the two cases, while $Au_2(C_2D_4)(CD_4)^+$ is absent in limiting case 1. (Top panel) TOF spectra at $[CD_4] = 3.1 \times 10^{13}$ cm^{-3}. Regions that would contain $Au_2(C_2D_4)^+$ (m/z = 426 Da) and $Au_2(C_2D_4)(CD_4)^+$ (m/z = 446 Da) (blue arrows) are shown multiplied by a factor of 10 to indicate that no peaks above the noise level of the experiment are apparent.

c)
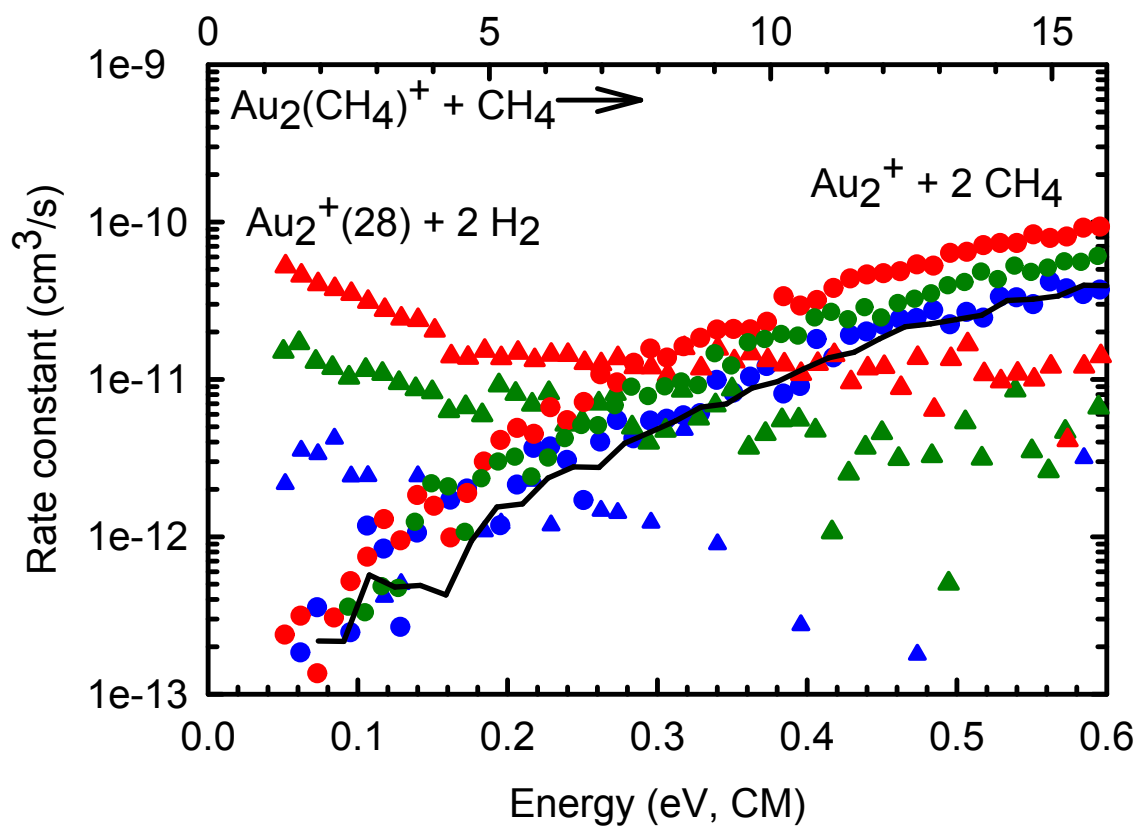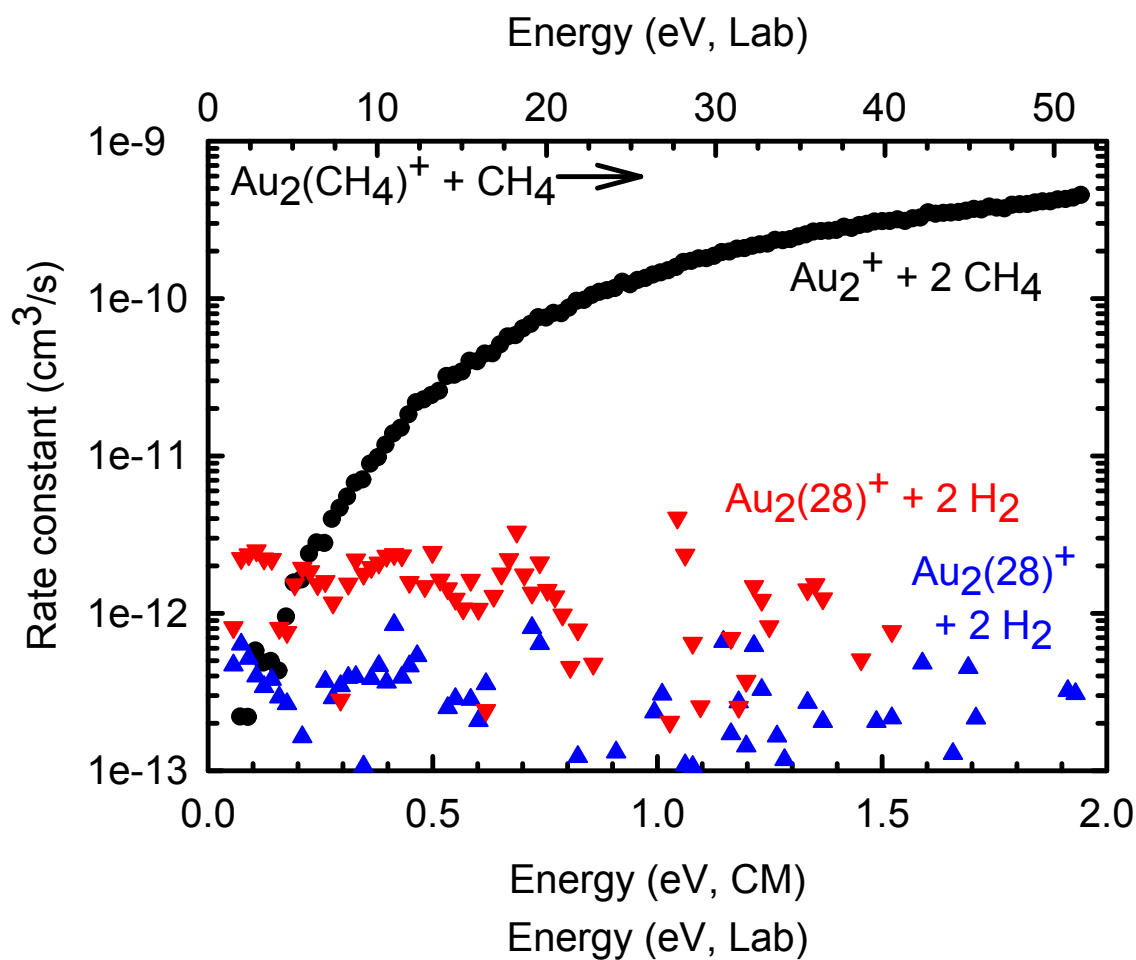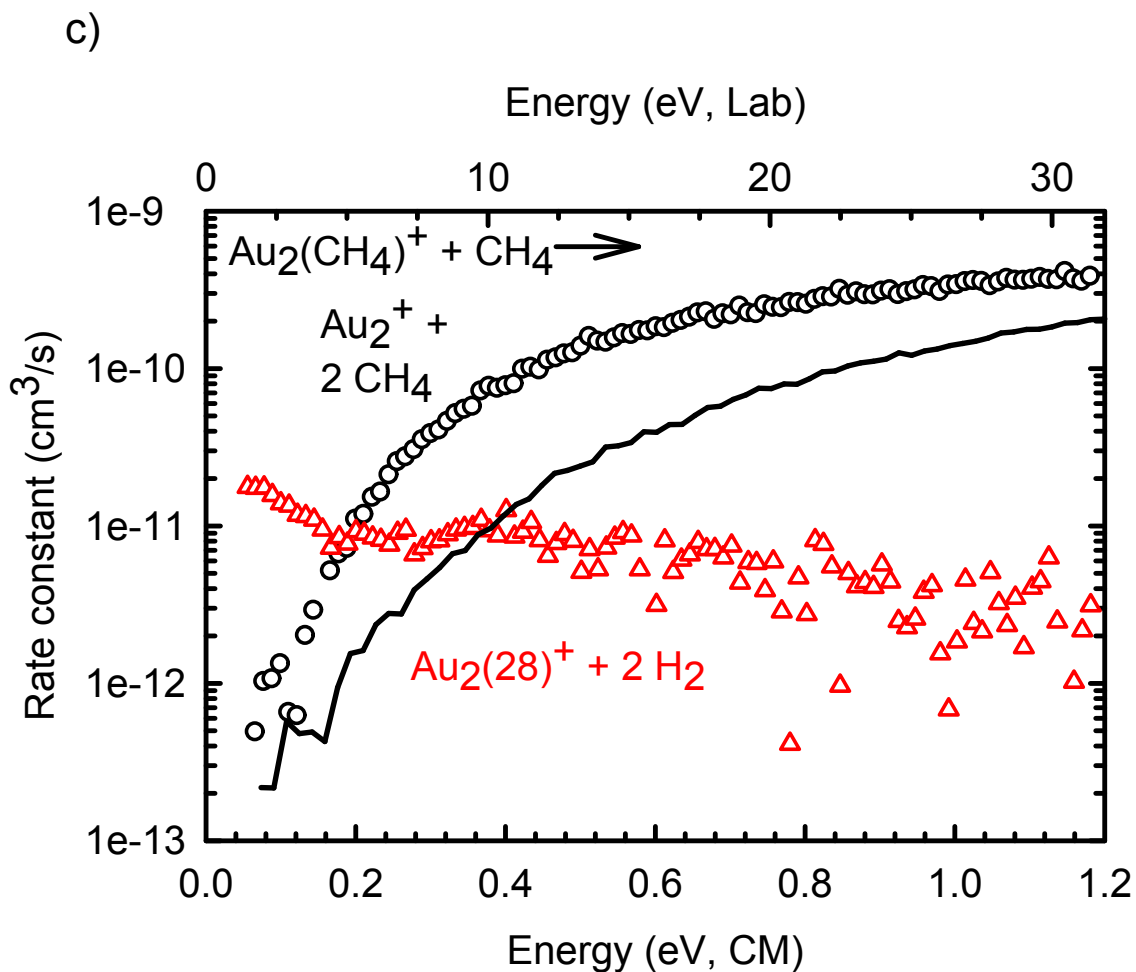
Figure 3. Rate constants for $Au_2(CH_4)^+ + CH_4$ as a function of kinetic energy in the center-of-mass (lower x-axis) and laboratory (upper x-axis) frames measured using the GIBMS. In part a, $Au_2^+(28)$ signals (red and blue) collected on different days under nominally identical conditions are shown. Part b shows similar data taken on another day with a fresh Au sample. Circles and triangles show data for reactions (6) and (7), respectively, with red, green, and blue data showing data sets taken sequentially over the course of about 2 hours. Part c shows data taken with O_2 in the source. In both parts b and c, the black line shows the rate constant measured for Au_2^+ products from part a.
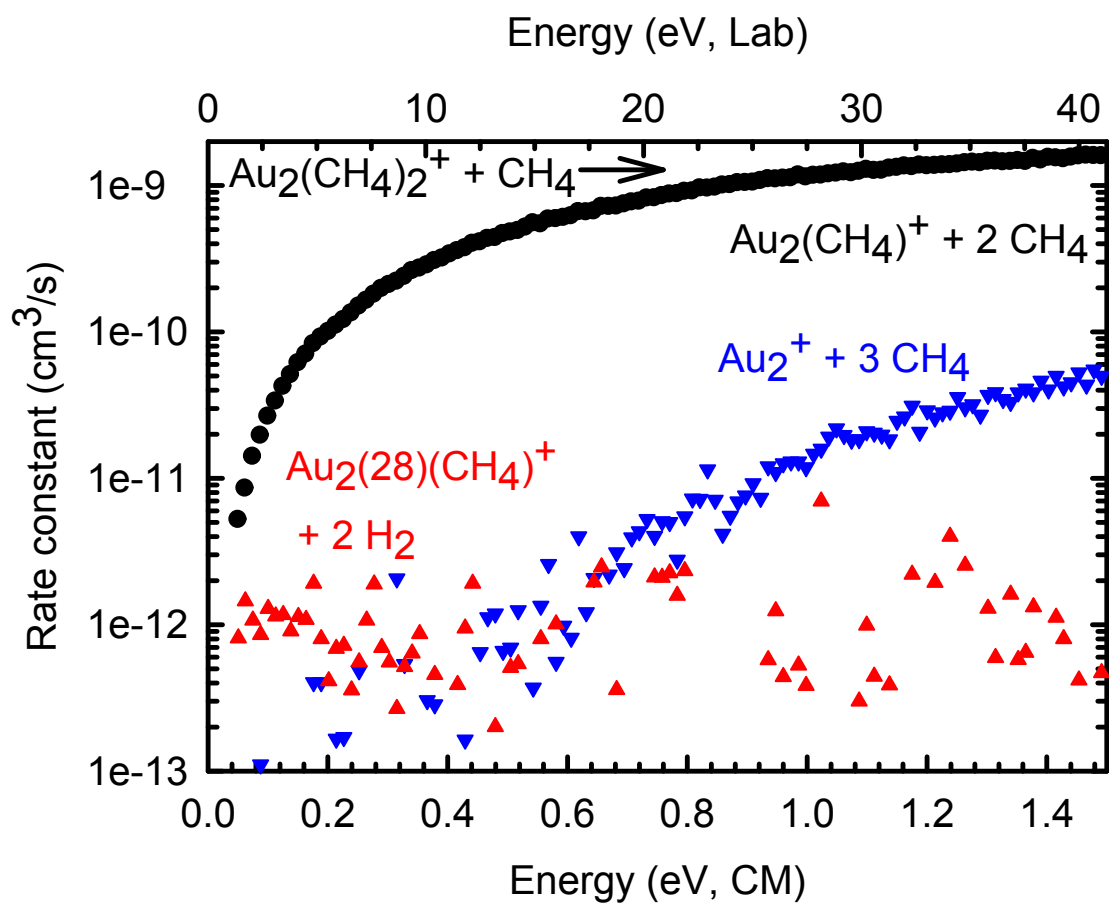
Figure 4. Rate constants for $Au_2(CH_4)_2^+ + CH_4$ as a function of kinetic energy in the center-of-mass (lower x-axis) and laboratory (upper x-axis) frames measured using the GIBMS.
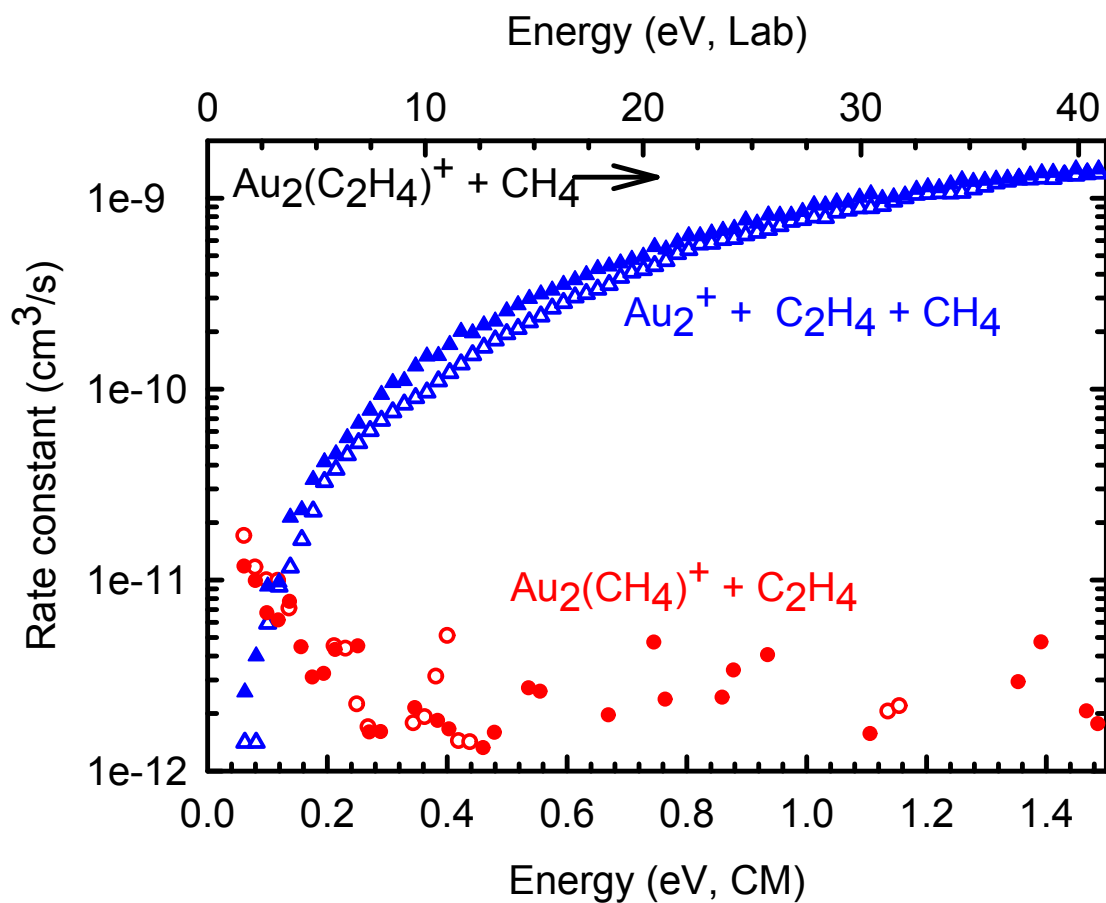
Figure 5. Rate constants for $Au_2(C_2H_4)^+ + CH_4$ as a function of kinetic energy in the center-of-mass (lower x-axis) and laboratory (upper x-axis) frames measured using the GIBMS. Open and closed symbols show two independent data sets.
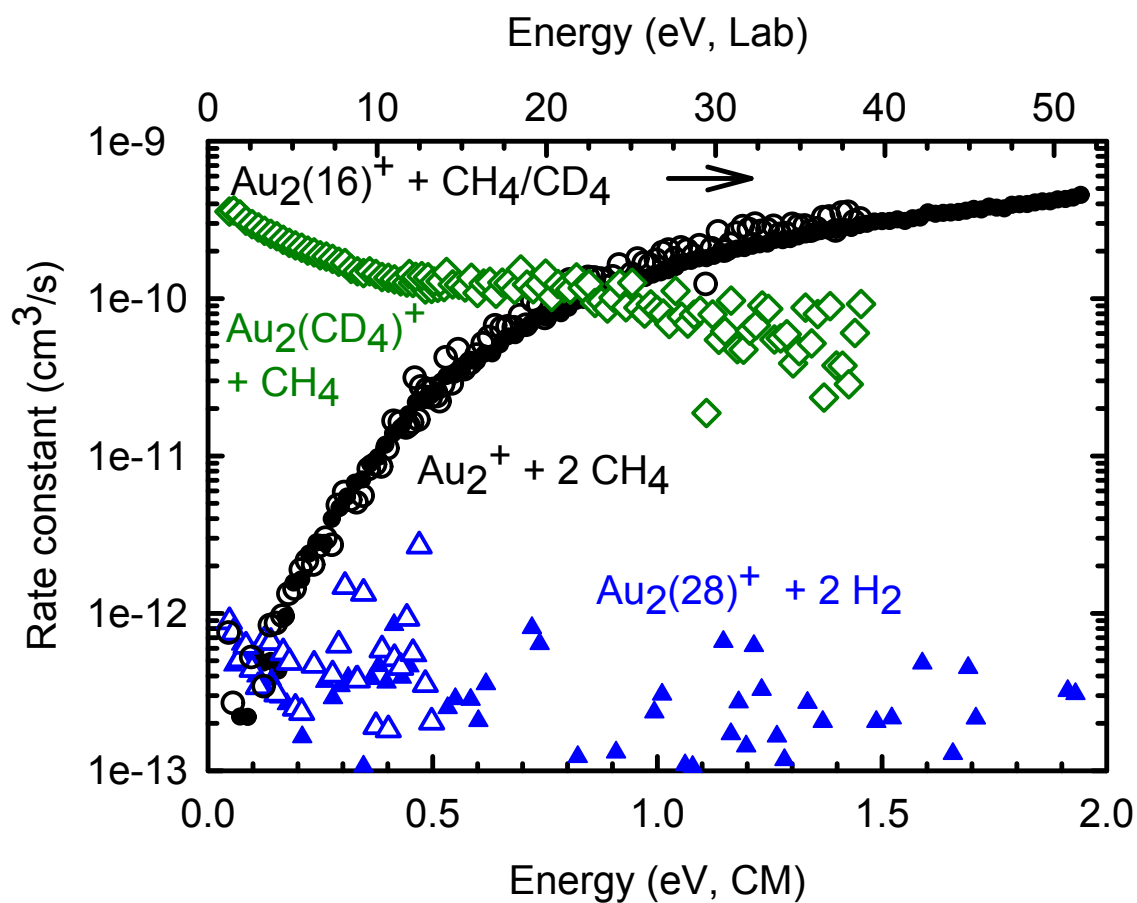
Figure 6. Rate constants for $Au_2(16)^+ + CH_4$ (closed symbols) and CD_4 (open symbols) as a function of kinetic energy in the center-of-mass (lower x-axis) and laboratory (upper x-axis) frames measured using the GIBMS. Although collected, no signal at $Au_2(30)^+$ was observed in the CD_4 experiments.
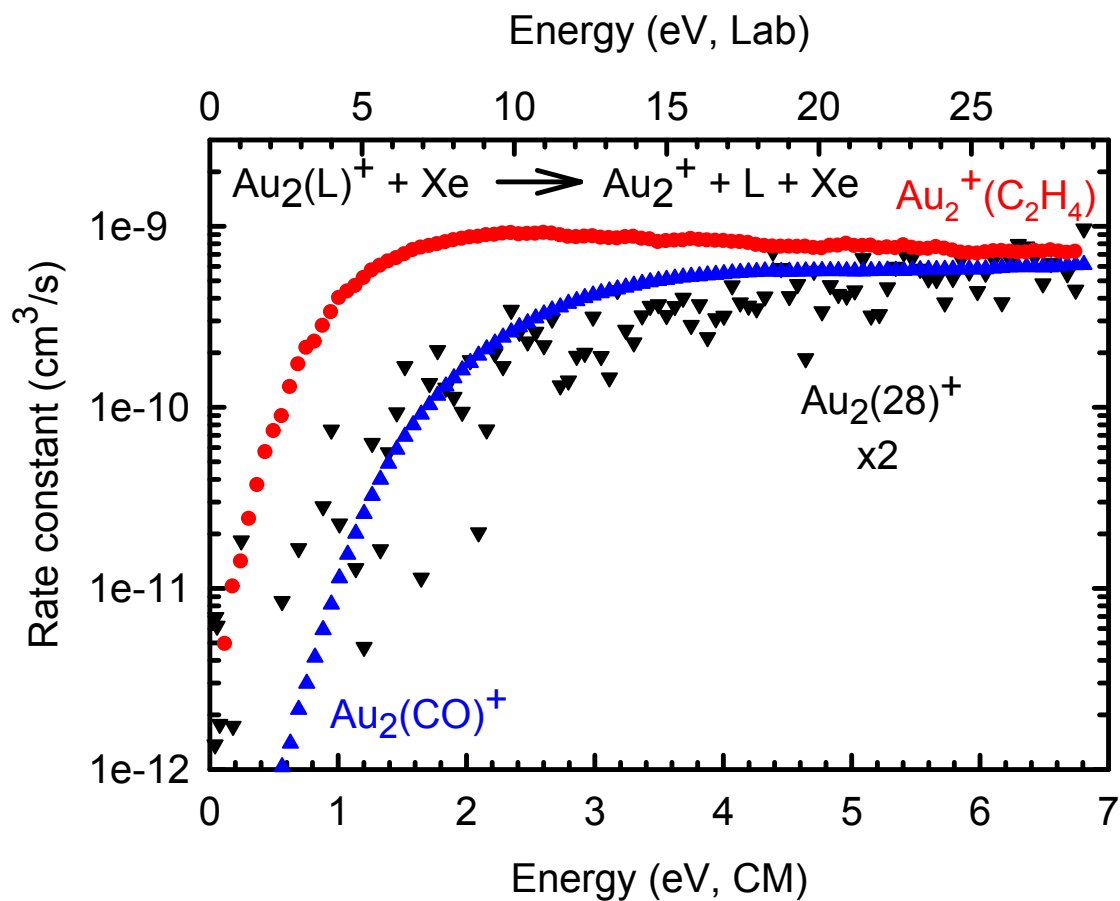
Figure 7. Rate constants for $Au_2(L)^+$ + Xe as a function of kinetic energy in the center-of-mass (lower x-axis) and laboratory (upper x-axis) frames measured using the GIBMS. Data are shown for three isobaric ions (m/z 422) formed with ethene in the source (red circles), carbon monoxide in the source (blue triangles), or methane in the source (black inverted triangles).
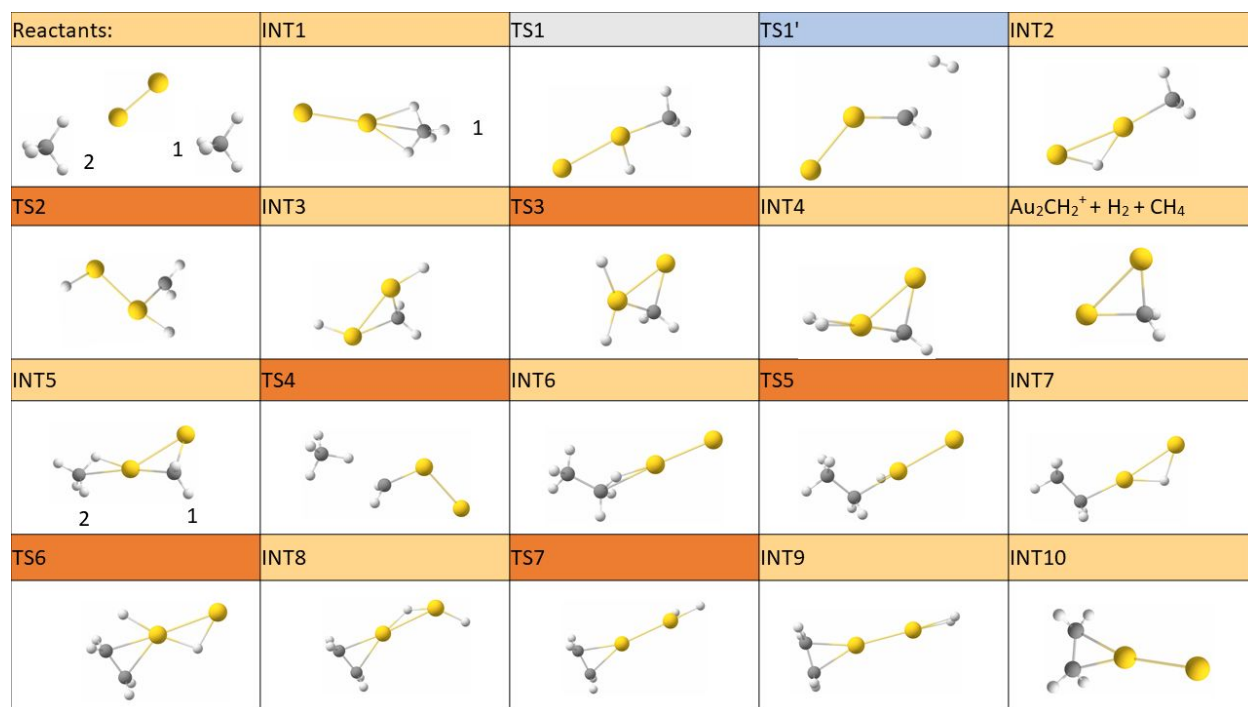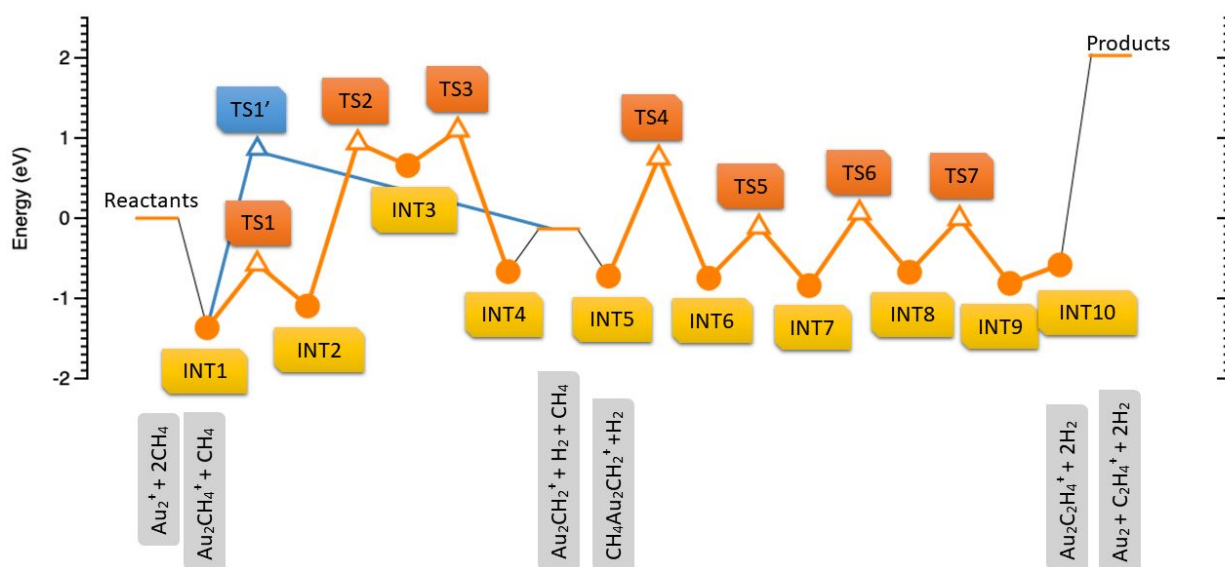
Figure 8. Reaction coordinates for $Au_2^+ + 2\,CH_4$ calculated at the B3LYP/def2-TZVPP level of theory. Zero-point corrected energies are shown relative to separated reactants. Structures of all stationary points are shown in the lower panel. Color scheme: Au: yellow, C: gray, H: white.